Journal for ImmunoTherapy of Cancer

Anti-HER2×CCR4 bispecific antibody enhances antitumor immunity in advanced HER2-positive tumors by chemotaxis blockade and depletion of tumor-associated Tregs, without inducing systemic toxicity

Chaokun Wang, Jiachang Li, Yue Tong, Haotian Chang, Jingyi Xu, Hanchen Zhu, Yongmei Yin, Meng Meng, Rimo Xi

To cite: Wang C, Li J, Tong Y, *et al*. Anti-HER2×CCR4 bispecific antibody enhances antitumor immunity in advanced HER2-positive tumors by chemotaxis blockade and depletion of tumor-associated Tregs, without inducing systemic toxicity. *Journal for ImmunoTherapy of Cancer* 2025;**13**:e012829. doi:10.1136/jitc-2025-012829

► Additional supplemental material is published online only. To view, please visit the journal online (https://doi.org/10.1136/jitc-2025-012829).

Accepted 01 December 2025

Nankai University, Tianjin, China

Correspondence to
Dr Rimo Xi;
xirimo@nankai.edu.cn

ABSTRACT

Background CCR4$^+$ regulatory T cells (Tregs), which are widely present in peripheral circulation and tumor microenvironment (TME), promote tumor immune evasion by infiltrating human epidermal growth factor receptor 2-positive (HER2$^+$) tumors in a chemokine-driven manner. However, therapies targeting CCR4 (eg, mogamulizumab) for systemic Treg depletion risk significant toxicity and have far been confined to hematological malignancies. Notably, tumor-chemotactic peripheral Tregs—key precursors to tumor-infiltrating Tregs (tumor-infiltrating lymphocyte (TIL)-Tregs)—remain overlooked.

Methods We designed and expressed four candidate anti-HER2×CCR4 DVD-Ig bispecific antibodies with varying degrees of anti-CCR4 domain masking, while leaving anti-HER2 domains fully exposed, to preferentially deplete tumor-associated Tregs, including TIL-Tregs and tumor-chemotactic peripheral Tregs. Stability and antitumor activity were assessed in vitro. In human immune system-reconstituted NOG mice, we systematically: (1) conducted a comprehensive dose-response evaluation of the XL-11 to characterize pharmacological efficacy and potential systemic toxicity, (2) assessed the immune memory, (3) studied the synergy of XL-11 with programmed cell death protein-1/programmed death-ligand 1 (PD-1/L1) blocker, and (4) analyzed pharmacokinetic profile (PK).

Results The lower affinity for CCR4 compared with HER2 enables anti-HER2×CCR4 DVD-Igs to priority target TIL-Tregs, and reduce binding to peripheral Tregs compared with mogamulizumab. Anti-HER2×CCR4 DVD-Igs inhibit Treg chemotaxis to TME, and killing Tregs and HER2$^+$ tumor cells through antibody-dependent cellular cytotoxicity. Among the candidates, XL-11, which had the greatest exposure of the anti-CCR4 domain, was selected for in vivo evaluation due to its superior stability and potent antitumor activity. In vivo models of gastric cancer and breast cancer, XL-11, by reducing TIL-Tregs and increasing CD8$^+$/Tregs ratios, induces potent antitumor activity even in advanced stages, with no evidence of metastasis. Concurrently, XL-11 specifically depletes tumor-chemotactic peripheral Tregs, further enhancing

WHAT IS ALREADY KNOWN ON THIS TOPIC

⇒ Regulatory T cells (Treg) depletion is a promising cancer immunotherapy strategy especially in human epidermal growth factor receptor 2 (HER2)$^+$ tumors; however, specifically eliminating Tregs remains challenging. Tumor-chemotactic peripheral Tregs—key precursors to tumor-infiltrating lymphocyte-Tregs—have been overlooked by current immunotherapies. CCR4 is essential for Treg migration, the effectiveness of mogamulizumab against solid tumors has not been conclusively shown, and its use is associated with systemic toxicity.

WHAT THIS STUDY ADDS

⇒ A novel tetravalent anti-HER2×CCR4 bispecific antibody XL-11 is presented that allows for specifically deplete tumor-associated Tregs in an HER2-directed manner. Furthermore, we established a novel animal model supporting lymphoid, myeloid, and natural killer cell coexistence, and providing comprehensive preclinical testing for XL-11. XL-11 demonstrated effective inhibition of tumor growth and metastasis in advanced HER2$^+$ tumors, with absence of systemic toxicity following prolonged or high-dose treatment due to XL-11 reducing peripheral CCR4$^+$ Tregs to physiological levels instead of causing Tregs exhaustion. XL-11 also acts synergistically with anti-programmed cell death protein-1 (PD-1) therapy, and exhibits favorable stability and pharmacokinetic (PK) supporting clinical translation.

HOW THIS STUDY MIGHT AFFECT RESEARCH, PRACTICE OR POLICY

⇒ We have proposed a promising strategy for advanced HER2$^+$ malignancies. This work advances Treg-targeted therapies, broadens the application of mogamulizumab, and enhances the effect of anti-PD-1 antibodies on tumors.

antitumor immunity while avoiding reducing Tregs throughout the body even at a high dose (10 mg/kg). There was no increase in memory T cells. In addition, XL-11 enhances the antitumor activity of anti-PD-1 antibodies and shows superior PK properties.

Conclusions XL-11 mediates potent antitumor immunity in advanced HER2$^+$ tumors while avoiding reducing Tregs throughout the body. XL-11 also acts synergistically with anti-PD-1 therapy, and exhibits favorable stability and PK supporting clinical translation. This work advances Treg-targeted therapies in HER2$^+$ tumors and overcomes the therapeutic limitations of mogamulizumab.

BACKGROUND

Advanced human epidermal growth factor receptor 2-positive (HER2$^+$) tumors, including breast, gastric, and non-small cell lung cancers, are characterized by increased metastasis and therapy resistance.[1 2] While immunotherapy, particularly anti-programmed cell death protein-1 (PD-1)/programmed death-ligand 1 (PD-L1) therapies combined with trastuzumab or chemotherapy, shows promising results in clinical trials, response rates remain modest (typically 10–15%).[3] This limited efficacy is partly attributed to immunosuppressive tumor microenvironment (TME).[4] Future strategies aim to incorporate novel immunomodulators and optimize combination therapies to improve therapeutic outcomes.

Regulatory T cells (Tregs), suppressive cells that drive tumor immune evasion, accumulate in the peripheral blood of patients with cancer and are enriched within tumor-infiltrating lymphocytes (TILs).[5] The chemokine receptor CCR4, expressed on the surface of Tregs, mediates Tregs chemotaxis toward TME-secreted CCL17/CCL22, recruiting peripheral CCR4$^+$ Tregs into the TME.[6] CCR4$^+$ TIL-Tregs suppress effector T cells (Teff cells) through inhibitory cytokines (eg, interleukin (IL)-10, transforming growth factor-beta (TGF-β)) and cell-contact mechanisms.[7 8] Treg infiltration inversely correlates with clinical outcomes. In HER2$^+$ tumors,[9] emphasizing the therapeutic potential of depleting CCR4$^+$ TIL-Tregs. Notably, tumor-chemotactic peripheral Tregs, characterized by high levels of CCR4 expression, exhibit tumor-specific enrichment and enhanced immunosuppressive capacity, making them become high-priority therapeutic targets.[10 11] In this study, TIL-Tregs and tumor-chemotactic peripheral Tregs are referred to as tumor-associated Tregs.

While CCR4-targeted Treg therapies have demonstrated clinical efficacy,[12] they face two challenges: (1) non-selective depletion risks systemic toxicity,[13] and (2) failure to address tumor-chemotactic peripheral Tregs—key precursors for TIL-Treg replenishment.[14–18] To overcome these limitations, spatially restricted strategies are needed to eliminate tumor-associated Tregs without affecting normal Treg function.

Bispecific antibody (BsAb) enables dual antigen targeting with tunable affinity for precision therapy.[19 20] In this study, we developed four anti-HER2×CCR4 DVD-Igs featuring differential masking of anti-CCR4 domains while fully exposing anti-HER2 domains. This design depletes tumor-associated Tregs while sparing systemic Tregs. Among the candidates, XL-11 demonstrates the most potent antitumor efficacy in vitro. In vivo, XL-11 demonstrates effective antitumor immunity without systemic toxicity, acts synergistically with anti-PD-1 therapy, and exhibits good stability and pharmacokinetic (PK), offering a translatable therapeutic strategy for advanced HER2$^+$ tumors.

METHODS

Generation and stability analysis of BsAbs

The variable regions of trastuzumab and mogamulizumab were used as the outer and inner domains of the DVD-Ig, respectively. The light chain variable regions were connected via linkers TVAAPSVFIFPP and TVAAP, and the heavy chain variable regions were linked with ASTKGPSVFPLAP and ASTKGP. Those variable regions were inserted into the vector pAb2c0-hCK and pAb20-hCHIgG1 (Synbio Technologies, China), respectively. The plasmids containing the heavy and light chain genes were co-transfected using PEI (FT401-01, TransGen Biotech, China) into HEK293F cells which were cultivated in the SMM 293-TII (M293TII, Sino Biological, China). Recombinant proteins were isolated using rProtein A beads gravity column (SA012GC01, SmartLifescience, China).

To assess thermal stability, ELISA plates were coated with HER2 (HE2-H5225, ACRO Biosystems, Beijing, China) or CCR4 (CSB-CF004843HU, CUSABIO, https://www.cusabio.cn) protein overnight at 4°C. After blocking with 5% bovine serum albumin (BSA), 1 hour heat-treated antibodies were added and incubated at 37°C. Following further washes, the plates were incubated with goat anti-human IgG-HRP (SE101, Beijing Solarbio Science & Technology), developed with 3, 3', 5, 5'-tetramethylbenzidine (TMB), and absorbance was measured at 450 nm.

Cell lines

Human cancer cell lines, MDA-MB-231, NCI-N87 and SKBR3, obtained from Procell, were cultured in RPMI-1640 or DMEM supplemented with 10% fetal bovine serum (FBS) and 1% penicillin/streptomycin (Gibco, USA). Cells were incubated at 37°C with 5% CO_2, while the medium pH was maintained at 7.2–7.4.

Surface plasmon resonance

Protein A and His chips were used to immobilize DVD-Ig and CCR4, respectively. HER2 and DVD-Ig, 500 nM initial concentration, twofold serial dilution served as analytes. The running buffer was phosphate-buffered saline (PBS) for HER2 experiments and PBS with 0.05% Fos-12 for CCR4 experiments. Regeneration was performed at 10 µL/min for 60 s using 10 mM glycine–HCl. Data were fitted using Biacore T200 software to determine the dissociation constant (Kd).

Indirect ELISA

HER2 and CCR4 antigens were coated onto plates. The next day, the plates were blocked with 5% BSA for 2 hours. Subsequently, serially diluted antibodies were added to the plates and incubated at 37°C for 2 hours. After the plates were washed, antibodies binding was detected using goat anti-human IgG-HRP. The absorbance values were read at 450 nm.

Ligand blocking ELISA

Human CCL22 (CSB-AP000951HU, CUSABIO, https://www.cusabio.cn) was coated onto plates. After the unbound CCL22 was removed, the plates were blocked with 5% BSA. Subsequently, the DVD-Ig and CCR4-His were mixed and added to the coated plates. Finally, antibodies binding was detected using anti-His antibody-HRP (BP5016-01, ACE). The absorbance values were read at 450 nm.

Cell binding assay

Cells were resuspended in flow cytometry buffer containing antibodies to be tested and incubated at 37°C for 1 hour. Unbound antibodies were washed off and incubated with goat anti-human IgG-Fc/FITC (SF105, Beijing Solarbio Science & Technology) for 30 min at 4°C. The data acquisition was performed on BD LSRFortessa and analyzed using FlowJo software.

Induction of Tregs in vitro

$CD4^+$ T cells were isolated from peripheral blood mononuclear cells (PBMCs) obtained from Milestone Biological Science & Technology, and then induced into Tregs using human Treg robust expansion kit (CT-011, Stemery Biotech, China). CCR4 fragments obtained from Synbio Technologies were transduced into Tregs to generate Treg-CCR4 cells.

DVD-Ig mediated co-binding assays

SKBR3 cells stained with carboxyfluorescein succinimidyl ester (CFSE) (S1076, Solarbio Science & Technology) and Treg-CCR4 cells stained with PKH26 (D0030, Solarbio Science & Technology) were mixed and incubated for 30 min in flow cytometry buffer containing the antibodies. The proportion of $CFSE^+$ $PKH26^+$ cells was assessed by flow cytometry. CFSE-stained SKBR3 cells were pre-fixed on confocal plates, and PKH26-stained Treg-CCR4 cells were co-cultured with the antibodies for 12 hours. After removing unbound cells, the co-binding of cells was observed under a confocal microscope (LSM 800 with Airyscan).

Antibody-dependent cellular cytotoxicity assay

The cytotoxic activity of antibodies was assessed using LDH cytotoxicity assay kit (KTA1030, Abbkine, Wuhan, China). PBMCs obtained from Milestone Biotechnologies were used as effector cells, with SKBR3, NCI-N87, or Treg-CCR4 cells as target cells, at an effector cells:target cells (E:T) ratio of 25:1. Maximum release was determined by adding 10% Triton X-100, while spontaneous and background release were measured using assay buffer in the presence of target cells alone or in cell-free wells, respectively. After 3 hours of incubation, the supernatant was incubated with lactate dehydrogenase (LDH) reaction solution for 30 min, and absorbance was measured at 565 nm. Cytotoxicity was calculated as follows: cytotoxicity% = ((experimental release − spontaneous release) / (maximum release − spontaneous release)) × 100.

Chemotaxis assay

Chemotaxis was assessed using well chambers (5 µm pore size). The medium in the upper chamber held Tregs and antibodies, while the lower chamber contained tumor culture medium supernatant with recombinant CCL22. After 4 hours at 37°C, the number of cells in the lower chamber was counted.

Regulatory T-cell suppression assay

$CD8^+$ T cells, as Teff, were acquired from Milestone Biotechnologies. Treg and CFSE-labeled Teff cells were co-cultured at a 1:4 ratio (Treg: Teff) in the presence of test antibodies for 48 hours. Tregs-mediated suppression of Teff cells proliferation was assessed by flow cytometry. The concentrations of interferon (IFN)-γ and IL-2 in culture medium supernatant were assessed using an ELISA kit (JL12152, JL19265-5, Shanghai Jianglai Biotechnology).

Stable cell clone establishment

MDA-MB-231-Luc cells and lentiviral particles were generated by Synbio Technologies. Human HER2 was cloned into the pCDH-CMV-MCS-EF1-Puro vector and transfected into 293T cells. Lentiviral particles were generated and used to treat MDA-MB-231-Luc cells. Stable cell clones were selected with puromycin. HER2 expression on MDA-MB-231-HER2-Luc cells was assessed by flow cytometry.

Construction of tumor models and human immune system in vivo

All mice were purchased from Vital River. Human $CD34^+$ HSC and PBMC were purchased from Milestone Biological Science & Technology. All mice experiments were conducted in compliance with protocols approved by the Nankai University Animal Care and Use Committee (Approval Number: 2024-SYDWLL-000770). All treatments (intraperitoneal injection) were administered every 6 days once tumor volumes reached approximately 100 mm^3. Tumor volumes and body weights were recorded every 3 days, with tumor volumes calculated as $(length \times width^2)/2$.

In therapeutic efficacy experiments of gastric cancer (NCI-N87) and breast cancer (MDA-MB-231-HER2-Luc), 6–8 weeks old female NOG (NOD/Shi-scid IL2Rγ$^{-/-}$) mice were irradiated (1.5 Gy) followed by immune reconstruction via tail vein injection with 5×10^4 human $CD34^+$ HSC. To expand natural killer (NK) cells, mice received daily intraperitoneal injections of 5 µg hIL-2 obtained from Sihuan Bioengineering for 7 days, and

2.5 µg hIL-15 obtained from Stemery Biotec every 5 days (three total injections). After 15 days, tumors were established by subcutaneous injection of NCI-N87 cells (3×10^6 cells/mouse) or orthotopic injection of MDA-MB-231-HER2-Luc cells (5×10^6 cells/mouse) which were mixed with Matrigel (082724, Mogengel Bio) in 1:1 ratio.

For comprehensive dose-response and combination therapy with anti-PD-1/PD-L1 (T9908, T9902 TargetMol, USA) assessments in the gastric cancer, 1 day before immune reconstitution (5×10^6 human PBMCs via tail vein injection), NOG mice were inoculated subcutaneously with NCI-N87 cells (3×10^6 cells/mouse and 5×10^6 cells/mouse) which were mixed with Matrigel in 1:1 ratio. To expand NK cells, on the day of PBMC injection, mice received intraperitoneal injections of 2 µg/mouse hIL-2 and 50 ng/mouse hIL-15 (every other day) for four times.

Flow cytometry analysis of samples from animals

Fresh blood was treated with erythrocyte lysis (E-CK-A105, Elabscience Biotechnology) for 10 min at 4°C. After centrifugation at 300× g for 5 min, the leukocyte pellet was collected for subsequent analysis. Tumor tissues were minced into 2–4 mm fragments and digested with DNA endonuclease, trypsin, and collagenase obtained from Solarbio at 37°C until complete dissolution. The isolated cell was passed through a 200-mesh nylon mesh, resuspended in staining buffer, and prepared for analysis. The fluorescent dyes obtained from Elabscience are listed in online supplemental table SI.

Living imaging

Following intraperitoneal injection of the D-fluorescein potassium salt (IL2330, Beijing Solarbio Science & Technology), a 15 min waiting period was maintained. Once mice were anesthetized with isoflurane gas, the mice were transferred to the imaging platform to ensure that the animals were comfortable and well-immobilized. The software (IVIS Spectrum) of the in vivo imaging system obtained the specific photon signal emitted by tumor cells.

H&E and IHC staining

For H&E staining, the nuclear was marked using 10% hematoxylin staining, and the cytoplasmic was marked using 1% eosin staining. For immunohistochemistry (IHC), antigen retrieval was performed using citrate buffer heated in a microwave oven. Endogenous peroxidase activity was blocked with 3% H_2O_2. Sections were incubated overnight at 4°C with primary antibody against target protein, followed by incubation with an HRP-conjugated secondary antibody. Signal was developed using DAB substrate, and sections were counterstained with hematoxylin.

PK analyses

XL-11 was administered via tail vein injection at 10 mg/kg to 8-week female C57BL/6J mice obtained from Vital River. Serum samples were collected at 5 min, 2 hours, 8 hours, 24 hours, 48 hours, 96 hours, 168 hours, 240 hours, 336 hours, and 504 hours post-dosing.

Statistical analyses

All analyses were conducted using GraphPad Prism V.7. All the experiments were performed with at least three independent biological replicates, and results were shown as means±SD. The Student's two-tailed t-test was used for statistical analysis. P values<0.05 were considered significant.

RESULTS

Analysis of CCR4 expression on Tregs from nat PBMCs, tumor PBMCs and TILs

To evaluate antitumor applicability of targeting HER2 and CCR4 simultaneously, we analyzed the CCR4 expression on Tregs from healthy mice PBMCs, cancer mice PBMCs and TILs. The Tregs, which accounted for approximately 2.13% of $CD4^+$ T cells in the nat PBMCs, had 49.8% expressing CCR4. The Tregs, which accounted for approximately 17.75% of $CD4^+$ T cells in the tumor PBMCs, had 87.9% expressing CCR4. The Tregs, which accounted for approximately 59.78% of $CD4^+$ T cells in the TILs, had 98.8% expressing CCR4 (figure 1A–D). These data demonstrate that Tregs are enriched in the tumor PBMCs and TILs. The $CCR4^+$ Tregs are the majority Tregs type in the tumor PBMCs and TILs. A significantly higher proportion of $CCR4^+$ cells in Tregs than $CD8^+$ T cells and conventional T cells (Tconv) (figure 1C,D) indicates that CCR4 may be a promising target for selective elimination of Tregs in the TILs.

The CCR4 is more highly expressed on TIL-Tregs (destination) than on Tregs of tumor PBMCs (source) (figure 1C,D), corroborating that Tregs can migrate to tumor sites when they gain more highly CCR4 expression in the peripheral circulation, which ultimately contributes to tumor immune escape. Thus, decreasing $CCR4^+$ Tregs in the peripheral circulation of tumor individuals also contributes to antitumor effect. Notably, approximately half of the Tregs from nat PBMCs are CCR4 positive (figure 1C,D), demonstrating that $CCR4^+$ Tregs have an important function under physiological conditions.

Anti-HER2×CCR4 DVD-Ig preferentially target TIL-Tregs

CCR4 blockers may cause systemic toxicity due to the exhaustion of peripheral Tregs essential for immune homeostasis.[21] To restrict antitumor activity to the tumor site, we developed a symmetric quadrivalent BsAb with one Fc region, two high-affinity external variable domains (VD1) targeting HER2 and two low-affinity internal variable domains (VD2) targeting CCR4. VD1 and VD2 are connected by two linkers designed as one long linker (L) and one short linker (S). To verify the effect of linker length on VD2 affinity and function, we constructed four anti-HER2×CCR4 DVD-Igs: XL-11 (L-L), XL-12 (L-S), XL-21 (S-L), and XL-22 (S-S) (figure 2A). The high

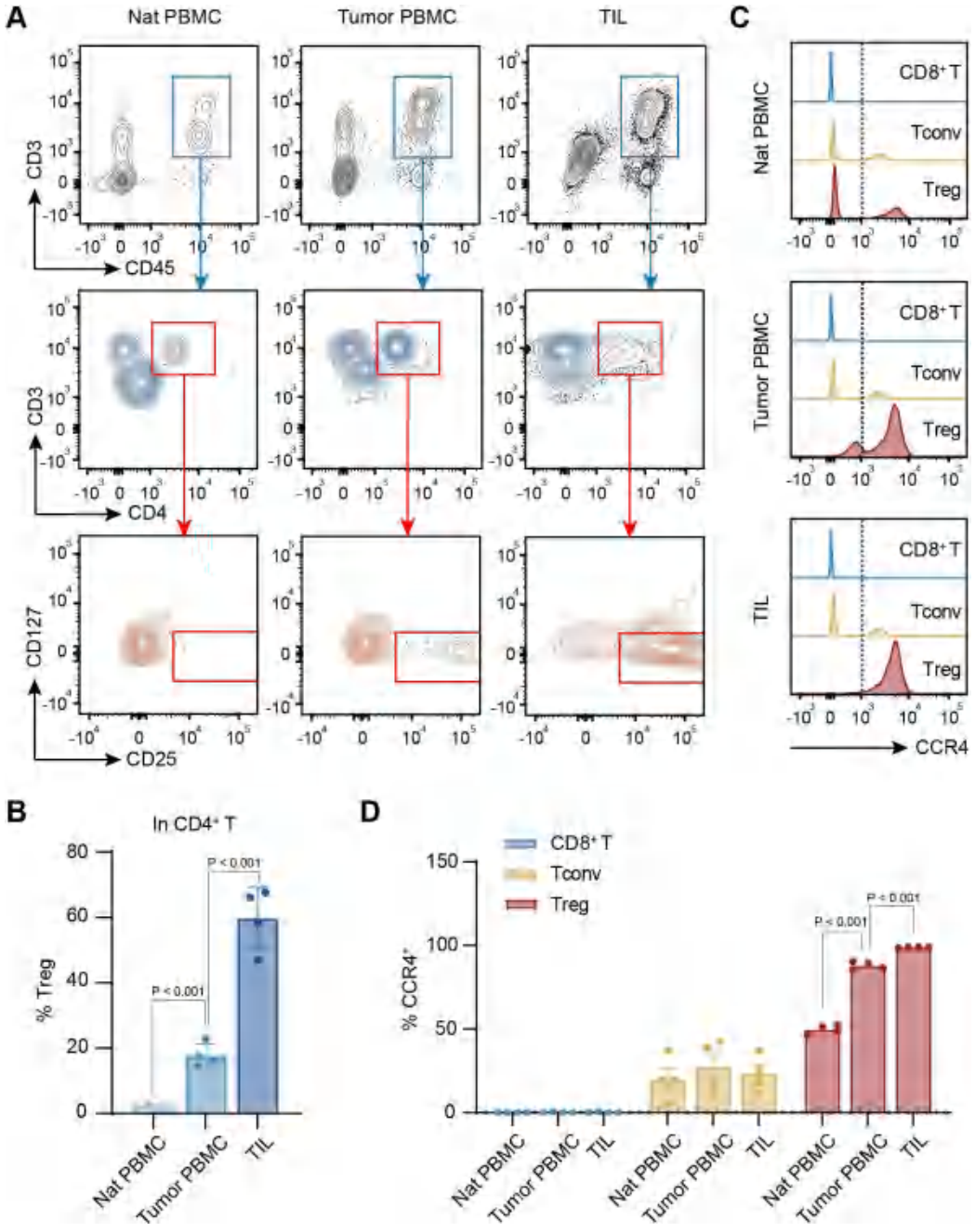

Figure 1 Flow cytometry analyses of CCR4 expression on Treg in NCI-N87 gastric cancer model. $CD8^+$ T cells ($CD3^+CD8^+$), Tconv ($CD3^+CD4^+CD25^-$) and Tregs ($CD3^+CD4^+CD25^+CD127^-$) were isolated from peripheral blood and TILs. (A) Representative flow cytometry plots. (B) Percentages of Tregs from nat PBMCs, tumor PBMCs and TILs. (C) Percentages of $CCR4^+$ cells on each T-cell subset from nat PBMCs, tumor PBMCs and TILs, representative histograms, with dotted lines indicating gating. (D) CCR4 expression on T-cell subsets in nat PBMCs, tumor PBMCs and TILs. Each data point represents a mouse sample, n=4. Values were expressed as mean±SEM. PBMC, peripheral blood mononuclear cell; Tconv, conventional T cell; TIL, tumor-infiltrating lymphocyte; Treg, regulatory T cell.

purity and correct structure of the four candidates were confirmed (figure 2B).

Surface plasmon resonance (SPR) indicated that DVD-Ig constructed did not reduce the affinity of VD1 compared with HER2 parental single-targeting antibody (α-HER2). All four candidates exhibited reduced affinity for CCR4 compared with the CCR4 parental single-targeting antibody (α-CCR4). Among them, XL-11 showed the highest affinity for CCR4, followed by XL-21, XL-12, and XL-22 (figure 2C and online supplemental figure S1). These conclusions were confirmed by ELISA (figure 2D,E). Furthermore, the four candidates exhibited lower affinity for CCR4 (EC_{50}=21.59 nM-1277 nM) than for HER2 (EC_{50}=5.772 nM-9.267 nM) (figure 2D,E), indicating enhanced selectivity for $HER2^+$ TIL-Tregs. Competitive ELISA results showed that the four candidates could block the binding of hCCL22 to CCR4, with XL-11 being the most effective (figure 2F). Flow cytometry

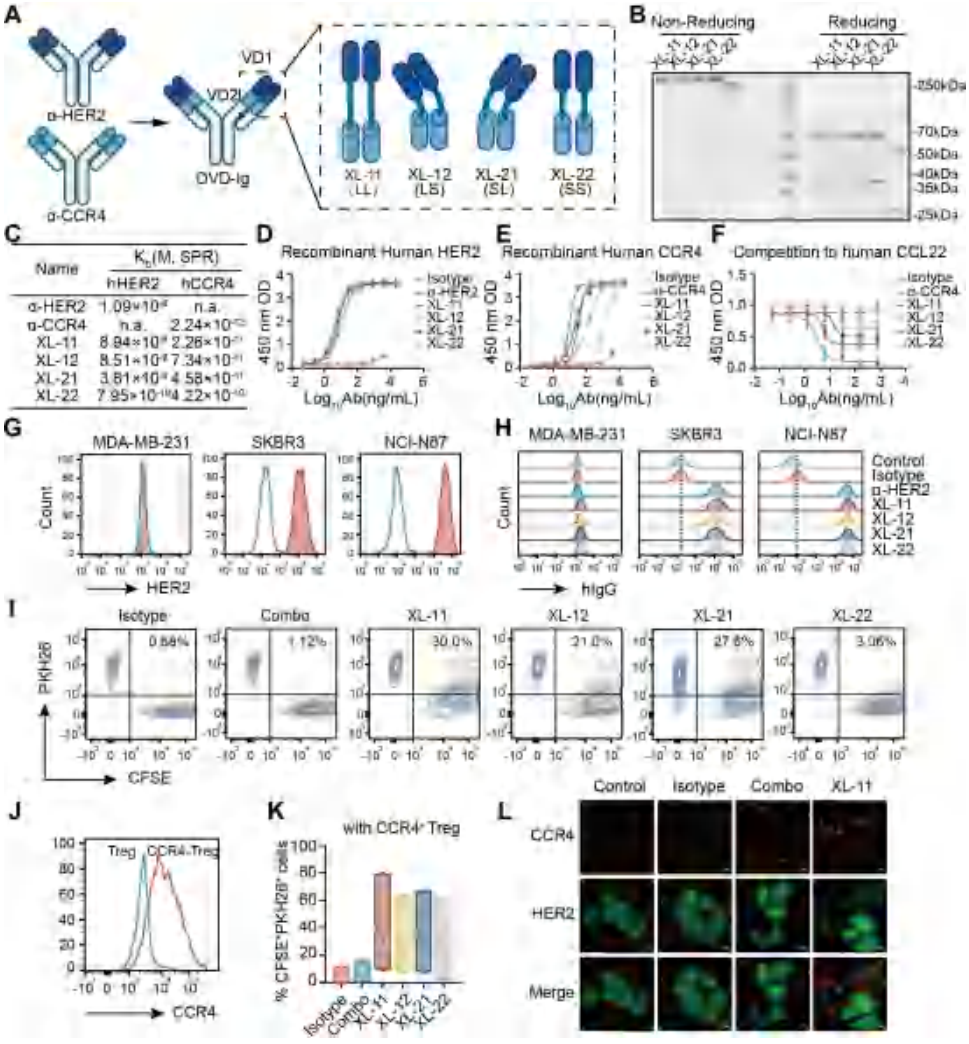

Figure 2 The structures and properties of four anti-HER2×CCR4 DVD-Igs. (A) Anti-HER2×CCR4 DVD-Igs consist of two VD1 and two VD2. The VD1 and VD2 are connected by linkers of different lengths. (B) SDS-PAGE gels of purified proteins under NR and R conditions determined the molecular weights of the anti-HER2×CCR4 DVD-Ig. (C) The affinity of anti-HER2×CCR4 DVD-Igs to HER2 and CCR4 protein was determined by SPR. (D, E) The affinity of anti-HER2×CCR4 DVD-Igs to HER2 protein (D) and CCR4 protein (E) was determined by ELISA. (F) Competitive ELISA was used to assess the competition of CCL22 protein and antibodies in binding to CCR4 protein. (G) Flow cytometry analysis of HER2 expression in MDA-MB-231 (left), SKBR (middle), and NCI-N87 (right) cells. (H) Flow cytometry analyzes the binding of anti-HER2×CCR4 DVD-Igs to MDA-MB-231 (left), SKBR (middle), and NCI-N87 (right) cells. Representative flow cytometry plots. (I) Representative flow cytometry plots. (J) CCR4 expression on Treg-CCR4 cells was assessed by flow cytometry. (K) Flow cytometry analyzed the HER2×CCR4 DVD-Ig mediated co-binding of SKBR3 cells and Treg-CCR4 cells by calculating $CFSE^+$ $PKH26^+$ populations. (L) Confocal microscopy was used to observe the co-binding of SKBR3 cells and Treg-CCR4 cells mediated by anti-HER2×CCR4 DVD-Ig. Green: $HER2^+$ cells, red: $CCR4^+$ cells. Microscope magnification: ×200 times. All in vitro experiments were performed three times independently. HER2, human epidermal growth factor receptor 2; SDS-PAGE, sodium dodecyl sulfate–polyacrylamide gel electrophoresis; SPR, surface plasmon resonance; Treg, regulatory T cell; VD, variable domains.

results showed that the binding of four candidates to three cell lines with low (MDA-MB-231), medium (SKBR3), and high (NCI-N87) HER2 expression (figure 2G), respectively, was similar to α-HER2, and the binding capacity was enhanced with the level of HER2 expression (figure 2H).

Treg-CCR4 cells were generated to serve as tumor-associated Tregs (figure 2J). Flow cytometry indicated that the four candidates could mediate the connection between $HER2^+$ cells and Treg-CCR4 cells; however, this phenomenon was not observed after incubation with α-HER2, α-CCR4, and Combo (figure 2I and K). This co-binding phenomenon can also be observed through laser confocal microscopy (figure 2L), which serves as the precondition for the function of antibodies within the TME.

XL-11 eliminates tumor-associated Tregs in vitro and prevents exhaustion of Tregs in the peripheral circulation

Given that the circulating and intratumoral $CCR4^+$ Tregs, via chemokine-driven infiltration, promoting tumor immune evasion by inhibiting Teff-mediated antitumor

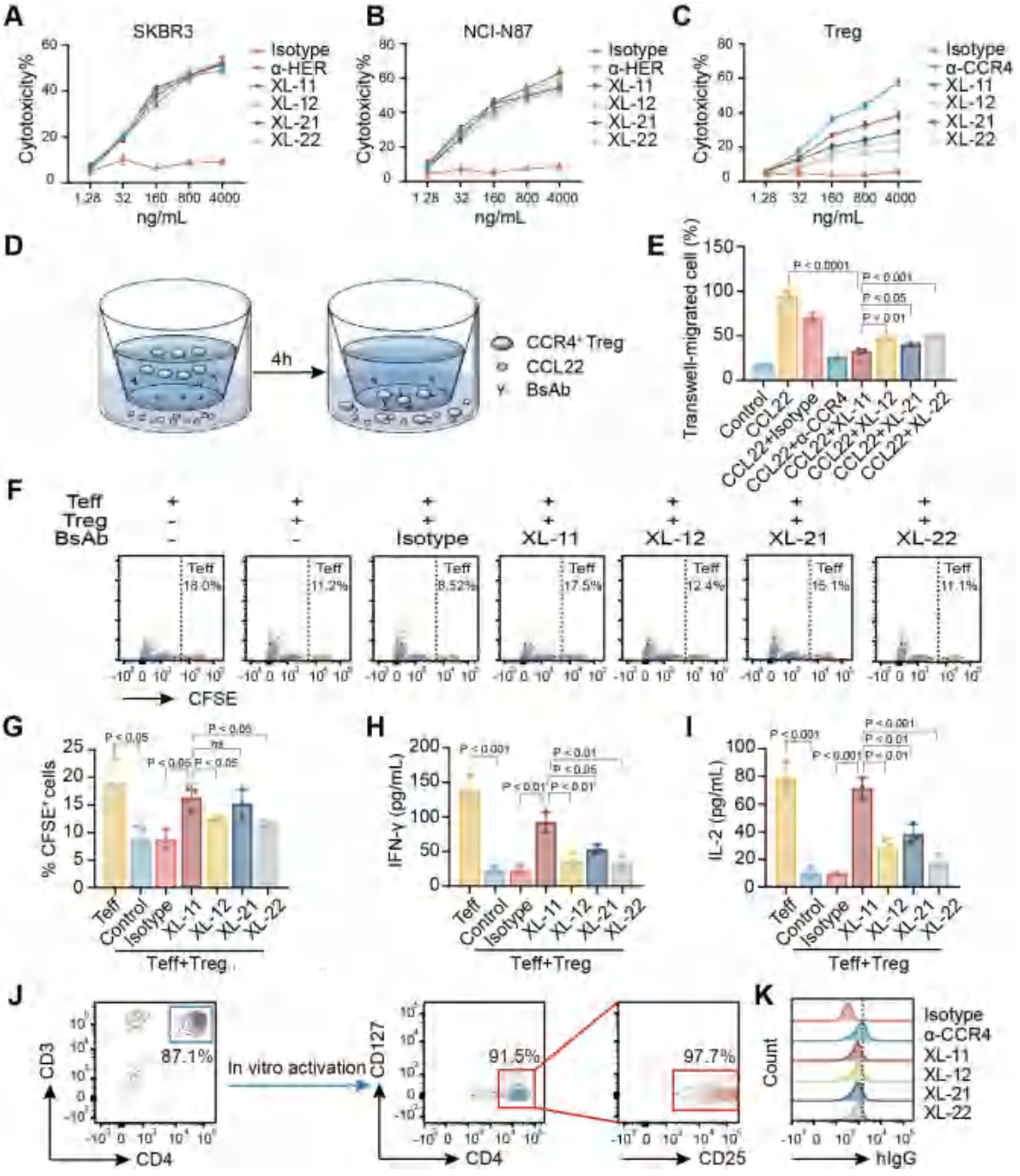

Figure 3 XL-11 eliminates tumor-associated Tregs in vitro and prevents the exhaustion of Tregs in the peripheral circulation. (A–C) The in vitro ADCC assays of SKBR3 (A), NCI-N87 (B), and Treg-CCR4 cells (C). (D) Schematic of chemotaxis assay. (E) Anti-HER2×CCR4 DVD-Ig inhibited CCL22 chemotaxis to Treg-CCR4$^+$ cells. (F–I) Teff cells were labeled with CFSE. The proportion of Teff cells was assessed by flow cytometry (F, G), and IFN-γ (H) and IL-2 (J) in the culture medium supernatant of the co-culture system was assessed by ELISA. (J) CD3$^+$ CD4$^+$ T cells from PBMC were isolated and differentiated to Tregs in vitro, and the proportion of CD3$^+$ CD4$^+$ T cells (left) and Tregs (middle, right) was assessed by flow cytometry. (K) The binding of anti-HER2×CCR4 DVD-Ig to Tregs was assessed by flow cytometry. All in vitro experiments were performed three times independently. Values were expressed as mean±SEM. ADCC, antibody-dependent cellular; CFSE, carboxyfluorescein succinimidyl ester; HER2, human epidermal growth factor receptor 2; IFN, interferon; IL, interleukin; PBMC, peripheral blood mononuclear cell; Teff, effector T cells; Treg, regulatory T cell.

immunity,[7] we attempted to identify a candidate with optimal antitumor activity.

At 4,000 ng/mL, the four candidates mediated the lysis of approximately half of tumor cells, similar to the α-HER2 (figure 3A,B). Compared with α-CCR4, the four candidates mediated varying degrees of Tregs killing, with the XL-11 mediating the strongest cytotoxicity, followed by XL-21, XL-12, and XL-22 (figure 3C). Chemotaxis

assay demonstrated that all candidates blocked CCL22-induced Treg migration, with XL-11 showing the greatest blocking ability, followed by XL-21, XL-12, and XL-22 (figure 3D,E). Separated Teff cells ($CD4^+$ Teff and $CD8^+$ Teff) were co-cultured with Tregs, the proliferation of Teff cells was inhibited, and the secretion of IFN-γ and IL-2 was significantly reduced. Treatment with the four candidates can overcome Treg-mediated immunosuppression and thereby enhance the Teff cell-mediated immune activation (figure 3F–I). Notably, XL-11 had a better activity to overcome Treg-mediated immunosuppression than other candidates.

To assess the safety of four candidates in the peripheral circulation, $CD4^+$ T cells were isolated from peripheral blood (purity >85%) and differentiated into Tregs (figure 3J). Those four candidates exhibited significantly reduced binding to peripheral circulating Tregs compared with α-CCR4 (figure 3K), implying a lower risk of systemic $CCR4^+$ Treg depletion. Among the four candidates, XL-11 was chosen for in vivo research due to its superior antitumor efficacy.

XL-11 effectively reduced tumor-associated Tregs in vivo

Based on previous research,[22–26] we transplanted human hematopoietic stem cells (huHSC-$CD34^+$) into NOG mice and treated with hIL-2 and hIL-15 to establish a mice model with a humanized immune system. Flow cytometry analysis using CD45 (leukocyte), CD56 and CD16 (NK cell) markers confirmed that this treatment significantly expanded the populations of human leukocytes and NK cells within 15 days, with no weight loss (figure 4A–F).

The antitumor efficacy of XL-11 was evaluated in HSC-NOG mouse models bearing NCI-N87 gastric cancer tumors (figure 4G). Compared with the control group (the mean tumor volume was 334.9 mm^3), while α-HER2, α-CCR4, and their combination only suppressed tumor growth (the mean tumor volumes were 202.6, 242.2 and 181.2 mm^3, respectively), XL-11 induced marked tumor regression, reducing the mean volume to 83.5 mm^3 (figure 4H–J). In addition, targeting the tumor directly (α-HER2) is more effective than immunosuppressive cell depletion (α-CCR4), and their combination demonstrates a synergistic effect. There were no adverse events or substantial weight loss among all treatment groups (figure 4K).

The composition of TILs determines whether it promotes immune evasion or antitumor immunity.[27] To elucidate the antitumor mechanism of XL-11, the frequency changes of $CD8^+$ T cells and Tregs in TILs were analyzed. XL-11's antitumor activity is primarily mediated by marked reduction in Tregs, which increased the $CD8^+$/Treg ratio, rather than by enhancing $CD8^+$ T-cell infiltration (figure 4L–N). Notably, although XL-11's VD2 exhibits weaker affinity than α-CCR4, XL-11 eliminated more intratumoral Tregs, potentially due to avoiding excessive exposure in systemic circulation. This was confirmed by analyzing peripheral $CCR4^+$ Tregs: α-CCR4 and Combo caused almost complete exhaustion of peripheral Tregs, whereas XL-11 achieved a significant reduction of peripheral Treg while maintaining their number within the physiological range (figure 4O,P).

XL-11 effectively suppressed the growth and metastasis of advanced $HER2^+$ tumor in vivo with no systemic toxicity

To assess the efficacy and potential systemic toxicity of XL-11 during prolonged treatment, the MDA-MB-231-HER2-Luc cells were used to generate an orthotopic metastasis tracking model (online supplemental figure S2). Long-term data collection (over 50 days) was performed until the mice exhibited severe graft-versus-host disease or death due to metastasis (figure 5A).

XL-11 exhibited superior and sustained antitumor activity, decreasing the mean tumor volume from 386.3 mm^3 to 111.8 mm^3, and almost halting tumor growth after 20 days, outperforming all other treatments (α-HER2: 303.6 mm^3, α-CCR4: 213.9 mm^3, Combo: 164.9 mm^3) (figure 5B–D). In the α-CCR4 group, half of the mice were observed to be arched back and lethargic, and even died, which can be divinable due to the over-depletion of Tregs. Only one mouse death in the Combo group, which is potentially attributable to the lower dose of α-CCR4. In contrast, there was no treatment-related death, significant weight loss and organ damage in the XL-11 group (figure 5B, E, F and G). In vivo imaging revealed that the 40th and 51st days after tumor transplantation, only XL-11-treated tumors did not show any signs of metastasis. All of the mice in the control and α-HER2 group died after 51 days due to the progression of cancer (figure 5H).

Our research findings indicate that XL-11 effectively inhibits the growth and metastasis of advanced $HER2^+$ tumor with a favorable safety profile.

XL-11 has good clinical translational potential

The comprehensive dose-response evaluation of XL-11 is essential for evaluating its clinical translational potential. We administered hIL-2 and hIL-15 to hPBMC-NOG mice to expand NK cells (online supplemental figure S3A–D). Mice bearing NCI-N87 tumor cells were treated with XL-11 at 1, 3, and 10 mg/kg (figure 6A). XL-11 treatment resulted in dose-dependent antitumor activity and intratumoral Tregs depletion (figure 6B–E, online supplemental S4A). A certain degree of tumor growth inhibition was observed even at the lowest dose (1 mg/kg). The high-dose (10 mg/kg) XL-11 reduced peripheral Tregs, while maintaining their number within the physiological range (figure 6F), without organ damage (online supplemental figure S5). We also assessed the proportion of memory T cells in peripheral blood (online supplemental figure S6A). While memory T cells were present in tumor-bearing mice, XL-11 treatment did not significantly alter its proportion, suggesting that XL-11 does not enhance the formation of immunological memory in this model (online supplemental figure S6B,C).

Given that overcoming the immunosuppressive TME is critical to improving the antitumor activity of immune

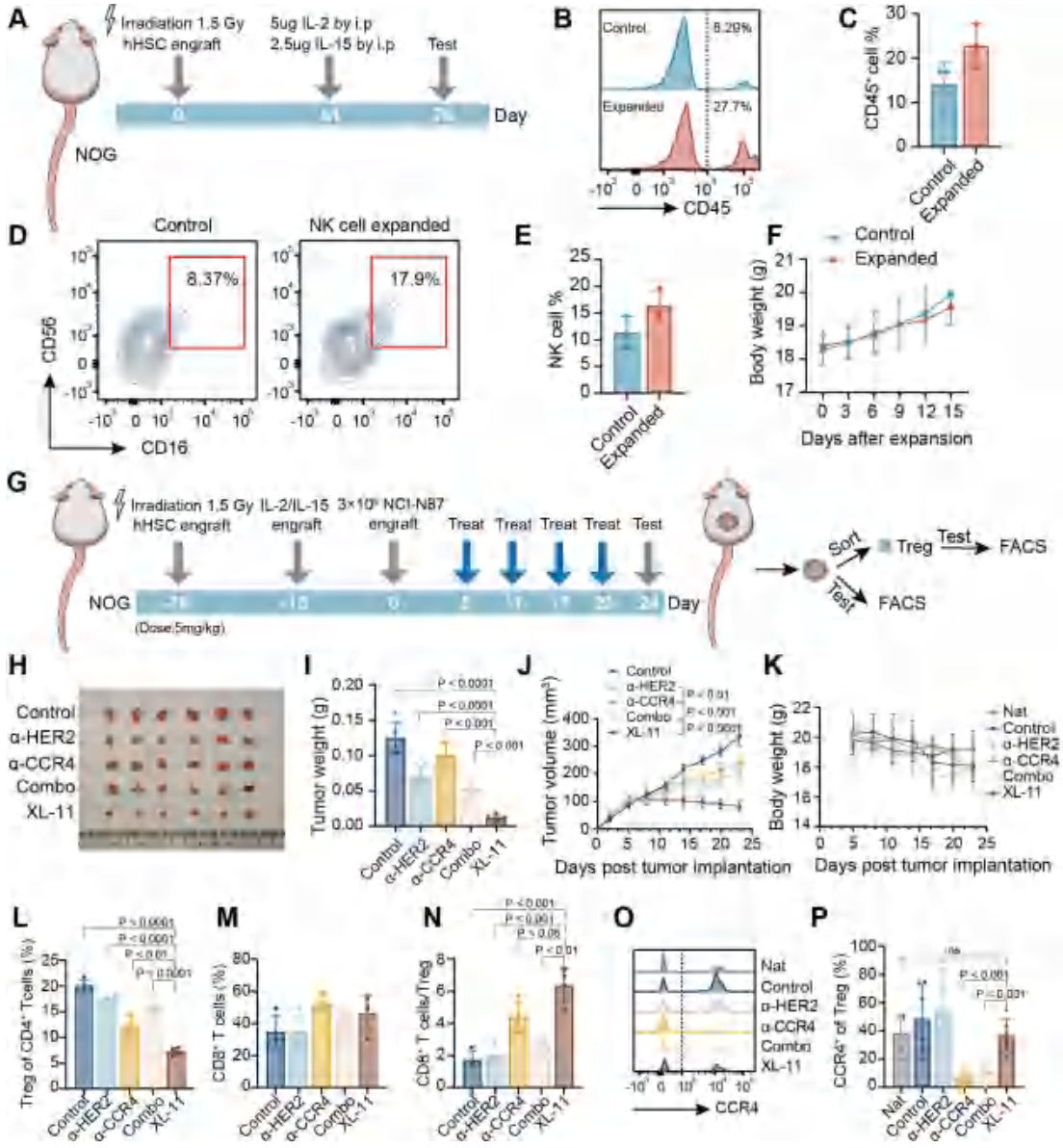

Figure 4 XL-11 effectively reduced tumor-associated Tregs in vivo. (A) Schematic representation of animal experiments. (B) Representative histogram of the proportion of leukocytes in the peripheral circulation, with dotted lines indicating gating. (C) The proportion of leukocytes in the peripheral circulation. (D) Representative flow cytometry plot. (E) The proportion of NK cells in the peripheral circulation. (F) The body weight of mice. Each data point represents a sample, n=3. (G) Schematic diagram of animal experiments. (H) Tumor mass. (I) Tumor weight. (J) Tumor growth curve. (K) Body weight of mice. (L) The percentage of Tregs in TILs in each group. (M) The percentage of $CD8^+$ T cells in TILs in each group. (N) The ratios of $CD8^+$/Tregs in TILs in each group. (O) Representative histograms of the percentage of $CCR4^+$ cells in Tregs in the peripheral circulation of each group, with dotted lines indicating gating. (P) The percentage of $CCR4^+$ cells in Tregs in the peripheral circulation of each group. Each data point represents a sample, n=6. Values were expressed as mean±SEM. FC, flow cytometry; HER2, human epidermal growth factor receptor 2; i.p., intraperitoneal; IL, interleukin; NK, natural killer; TIL, tumor-infiltrating lymphocyte; Treg, regulatory T cell.

checkpoint blockade, we evaluated the antitumor activity of XL-11 combined with PD-1/L1 blockers (figure 6G). Compared with the control group (mean tumor volume: 912.2 mm^3), the PD-1/L1 blockers have shown limited antitumor activity. XL-11 (272.2 mm^3) demonstrated superior efficacy to α-PD-1 (806.2 mm^3) or α-PD-L1 (698.7 mm^3) use alone. There was a strong synergistic effect when XL-11 combined with PD-1 blocker (mean tumor volume: 135.4 mm^3) without causing weight loss (figure 6H–K). This combination also enhanced $CD8^+$ T cells infiltration. A transition from "cold" to "hot" tumor was observed (figure 6L, online supplemental S4B). In contrast, the combination with α-PD-L1 was less effective (392.7 mm^3).

Table 1 The thermal melting temperature (T_m) is defined as the temperature at which 50% of antibodies after heat treatment still maintain their binding ability to the antigen molecules.

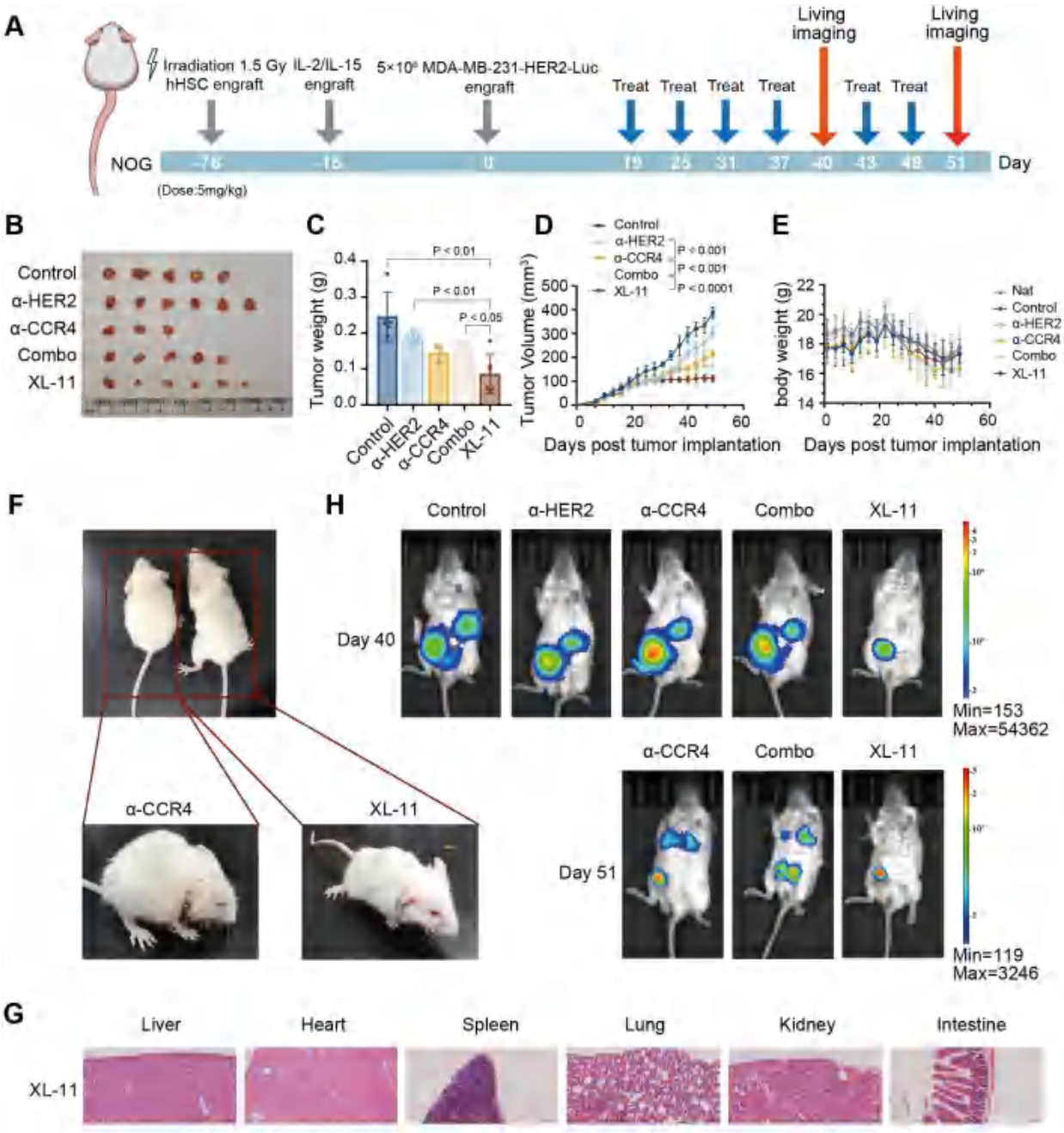

Figure 5 XL-11 effectively suppressed the growth and metastasis of advanced HER2$^+$ tumor in vivo with no systemic toxicity. (A) Schematic diagram of animal experiments. (B) Tumor mass. (C) Tumor weight. (D) Tumor growth curve. (E) Body weight of mice. (F) Representative images of mice. (G) Representative H&E staining images after XL-11 treatment, the scale bar was 0.1 mm. (H) In vivo imaging experiments assess breast cancer metastasis. Each data point represents a sample, n=6. Data were expressed as mean±SEM. HER2, human epidermal growth factor receptor 2; IL, interleukin.

Assessing the stability and PK of XL-11 is important to confirm its structural stability and bioactivity. Thermal stability assessment as figure 6M,N and table 1 revealed that the T_m for the anti-HER2 and anti-CCR4 domains of XL-11 were 62.89°C and 61.19°C, respectively. For comparison, the T_m of the parental antibodies trastuzumab and α-CCR4 were 72.59°C and 65.28°C. These results confirm that XL-11 exhibits good thermal stability. As figure 6O and table 2 revealed that XL-11 had a half-life of approximately 4.5 days.

DISCUSSION

Reducing Tregs is a promising approach in treating HER2-positive tumors.[28 29] Immunotherapy targeting Tregs has been studied in preclinical models and clinical trials of a variety of tumors with promising results.[30–32] However, it is still a challenge to find an efficient immunotherapy that can overcome Treg-mediated immunosuppression without side effects. In this study, we present the rational design of anti-HER2×CCR4 DVD-Ig XL-11. XL-11 takes advantage of the relatively high affinity to

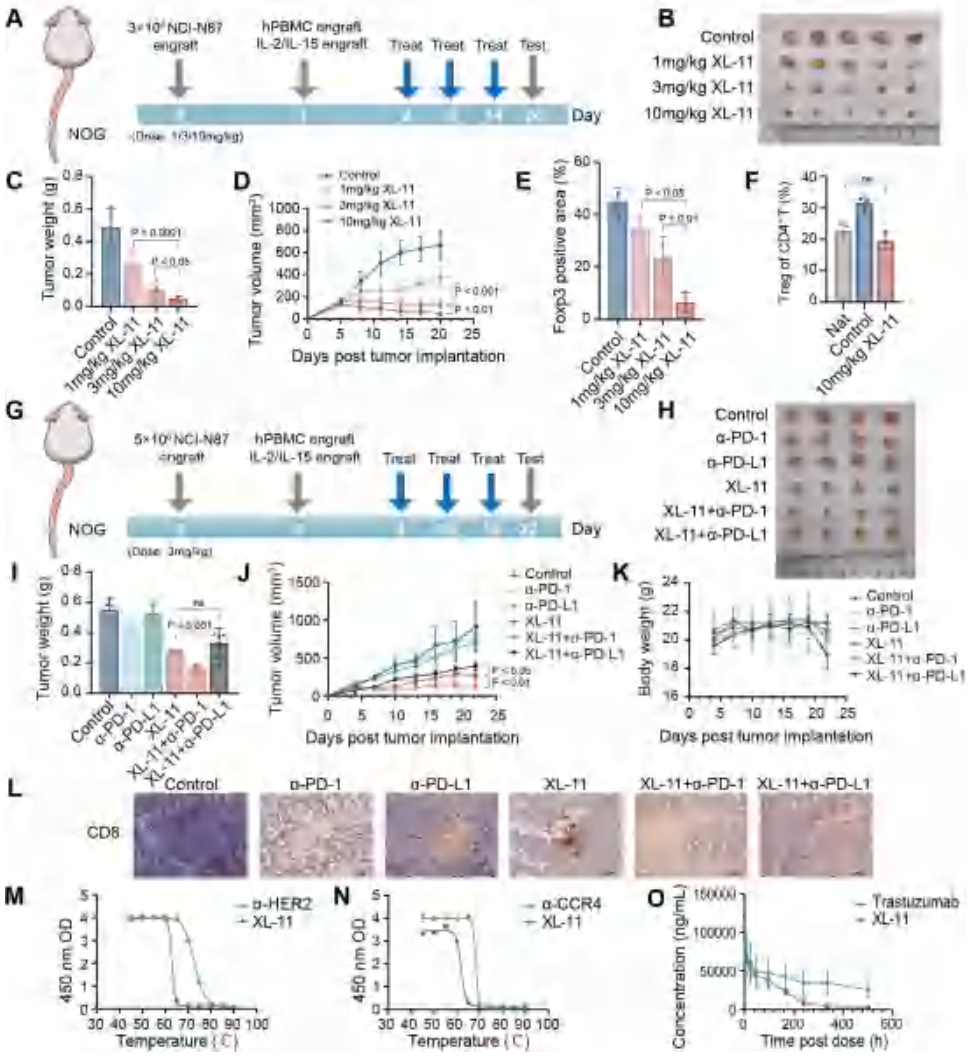

Figure 6 XL-11 has good clinical translational potential. (A) Schematic representation of comprehensive dose-response evaluation experiments. n=5. (B) Tumor mass. (C) Tumor weight. (D) Tumor growth curve. (E) The quantitative evaluation of Foxp3 positive area. (F) The percentage of Tregs in the peripheral circulation was assessed by flow cytometry. (G) Schematic representation of the study on synergistic effect of XL-11 and PD-1/L1 blocker. n=4. (H) Tumor mass. (I) Tumor weight. (J) Tumor growth curve. (K) Body weight of mice. (L) The immunohistochemical images of CD8 positive area, the scale bar was 0.2 mm. (M, N) The thermal stability assessment shows the binding of heated XL-11 to the HER2 (left) and CCR4 (right) protein. (O) The time-concentration curves following the first (2 hours) and last (day 21) intravenous administrations of 10 mg/kg XL-11. n=5. Values were expressed as mean±SEM. HER2, human epidermal growth factor receptor 2; IL, interleukin; PD-1, programmed cell death protein-1; PD-L1, programmed death-ligand 1; Treg, regulatory T cell.

HER2 on tumor and the modest affinity to CCR4 on tumor-associated Tregs to induce a potent antitumor effect through ADCC without causing obvious side effects by avoiding the exhaustion of Tregs essential for immune homeostasis in peripheral circulation.

Table 1 The thermal stability assessment

	Tm-HER2 (°C)	Tm-CCR4 (°C)
α-HER2	72.59	N/A
α-CCR4	N/A	65.28
XL-11	62.89	61.19

CCR4, C-C Chemokine Receptor type 4; HER2, human epidermal growth factor receptor 2; Tm, The thermal melting temperature.

Many studies have shown that the high level of Tregs is associated with poor prognosis of tumors.[33–35] Therefore, eliminating TIL-Tregs is important in enhancing antitumor effects. Denileukin-diftitox enables diphtheria toxin to enter the cell by binding to CD25 and killing Tregs. However, due to the universal expression of IL-2R on Teff cells, its application to other tumors treatment such as melanoma has been limited.[36] Similarly, ipilimumab binding CTLA-4 eliminates Tregs by the ADCC. However, it may increase the side effects on other immune cells.[37] Targeting TIL-Tregs while avoiding non-targeted tissues is difficult due to the widespread expression of markers on immune cells. Our data show that the delivery of CCR4 blocker by XL-11 to TIL-Tregs is effective and safe, which is partly due to CCR4$^+$ Tregs

Table 2 PK parameters of XL-11 after a single intravenous injection of 10 mg/kg into mice

	$t_{1/2}$ (hour)	AUC_{0-t} (hour×μg/mL)	$AUC_{0-\infty}$ (hour×μg/mL)	Vss (mL/kg)	CL (mL/hour/kg)	MRT_{0-t} (hour)	C_{max} (μg/mL)	T_{max} (hour)
Trastuzumab	440.65	18959.71	34065.78	5.41	0.008	214.75	87.07	0.08
XL-11	109.06	9246.25	9628.24	3.03	0.02	122.33	114.34	0.08

$AUC_{0-\infty}$, area under the serum concentration-time curve from time zero to infinity; AUC_{0-t}, area under the serum drug concentration-time curve up from time zero to the last measurable concentration; CL, total body clearance following vascular administration of the drug; C_{max}, maximum drug concentration observed in the serum; MRT_{0-t}, mean reaction time from time zero to the last measurable concentration; PK, pharmacokinetic; $t_{1/2}$, effective half-time; T_{max}, time of the first occurrence of C_{max}; Vss, apparent volume of distribution in the steady state.

being the predominant Tregs type in TILs and partly due to the moderate affinity of the XL-11's internal domain. Our in vivo experiments have shown that XL-11 is safer than α-CCR4. Other studies have also indicated that combining high-affinity and low-affinity approaches can minimize side effects. For example, using BiTE with lower CD3 affinity can reduce the risk of T-cell overactivation.[38] Similar designs are also demonstrated in blinatumomab and catumaxomab.[39 40]

Notably, previous studies have focused on eliminating TIL-Tregs, disregarding that increasing peripheral Tregs might enhance the metastatic potential of tumor cells.[41–43] It is another focus of Tregs-targeted therapy to precisely target tumor-chemotactic peripheral Tregs while avoiding the exhaustion of Tregs essential for immune homeostasis in peripheral circulation. Although XL-11 decreases the binding affinity of Tregs, it still retains the binding ability to the Tregs with higher CCR4 expression in the peripheral circulation. Furthermore, tumor-chemotactic peripheral Tregs, with higher CCR4 expression, are in the process of chemotaxis toward the TME, so it is easier to bind with XL-11. It has shown that XL-11 can reduce

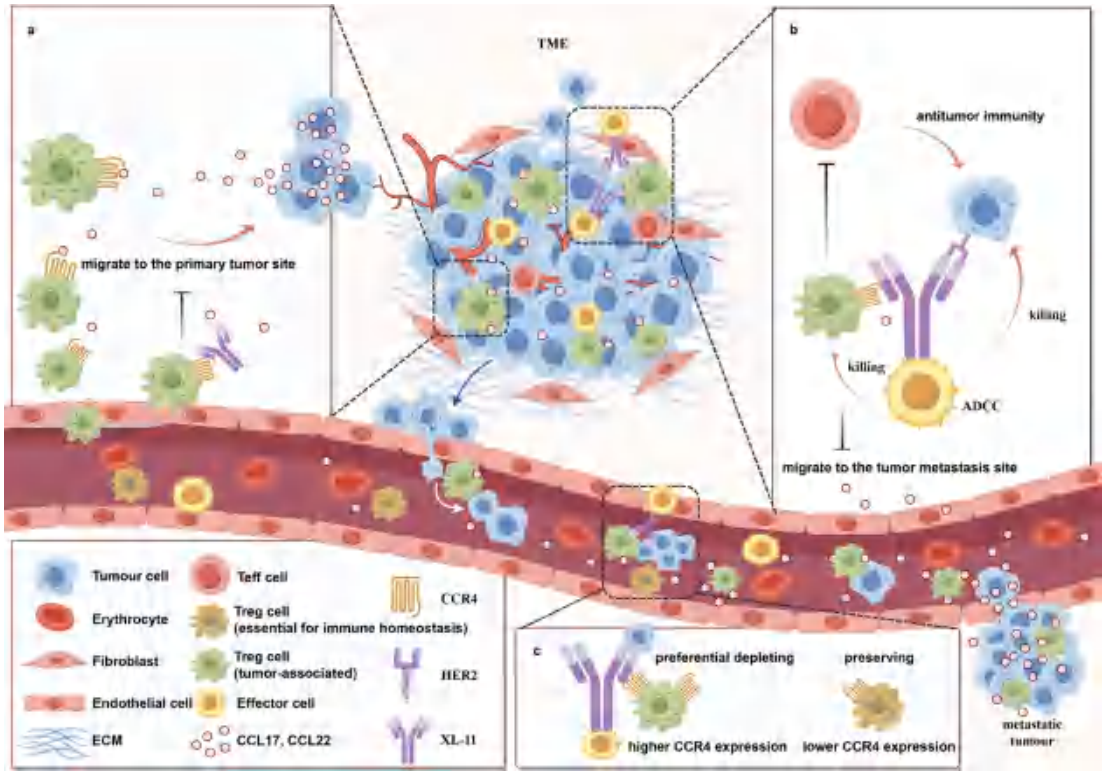

Figure 7 A schematic illustrating the mechanism of XL-11-mediated antitumor activity without systemic toxicity. (a) CCR4 ligands CCL22 and CCL17 establish a chemotactic microenvironment around the tumor, recruiting peripheral $CCR4^+$ Tregs into the TME. XL-11 inhibits CCL22/CCL17–CCR4 binding, suppressing Treg chemotaxis and infiltration into the TME. (b) XL-11 targets tumor cells and TIL-Tregs to eliminate these cells by inducing ADCC. This action overcomes TIL-Treg–mediated suppression and restores the function of Teff. Additionally, XL-11 prevents TIL-Treg migration to metastatic sites via CCR4 blockade. (c) XL-11 depletes tumor-chemotactic Tregs with high expression of CCR4 while maintaining Tregs essential for immune homeostasis in peripheral circulation. ADCC, antibody-dependent cellular cytotoxicity; ECM, extracellular matrix; HER2, human epidermal growth factor receptor 2; Teff, effector T cells; TIL, tumor-infiltrating lymphocyte; TME, tumor microenvironment; Treg, regulatory T cell.

tumor-chemotactic peripheral CCR4$^+$ Tregs and maintain the number of peripheral CCR4$^+$ Tregs at normal levels.

We also demonstrated the in vivo antitumor efficacy of XL-11 relying on the ADCC effect. The traditional PBMC-NOG mouse has a short window period,[23] which is not long enough to carry out research. The HSC-NOG mice have a long window period but lack NK cells. Therefore, there is no suitable animal model for in vivo study of antibodies that rely on ADCC to exert antitumor effect.[44 45] Previous research has shown that the cytokine-stimulated SCID mice have sufficient NK cells to support ADCC. Similar methods that use cytokine to expand NK cells have been reported in other mouse models.[24–26] In NK cells expanded HSC/PBMC-NOG mice, we demonstrated that XL-11 can effectively deplete tumor-associated Tregs, resulting in a potent and long-term antitumor activity in HER2$^+$ tumors, without systemic toxicity in prolonged/high-dose treatment.

Regarding antitumor activity, XL-11 specifically eliminates HER2$^+$ tumor cells and tumor-associated Tregs. Meanwhile, XL-11 can suppress the migration of peripheral Tregs to tumors, as well as the migration from primary tumor to metastatic sites, resulting in sustained effects on the growth and metastasis of advanced HER2$^+$ tumors. Regarding safety, XL-11 reduced peripheral Tregs to physiological levels rather than exhausted, thus avoiding systemic toxicity even in prolonged/high-dose treatment (figure 7). Regarding clinical translational potential, XL-11 exhibits wide therapeutic window, good thermal stability and PK parameters. Notably, XL-11 demonstrates strong synergistic effects with anti-PD-1 therapy and enhances its efficacy by converting "cold" tumors into "hot" tumors through increased CD8$^+$ T cells infiltration. In summary, XL-11 is a promising therapeutic strategy for advanced HER2$^+$ tumors.

Acknowledgements We would like to thank Dr. Haihong Ni and her team at Athena Pharma Inc. for helping in prioritizing the target selection of our bispecific antibody work. We would like to thank Sino Biological for the production of antibodies. We would like to thank Vital River for suggestions on the animal experiment. The structure and mechanism diagrams were created with authorized materials using FigDraw (ID: PUASTa9d25; YSWWW2ad7d).

Contributors CW: Conceptualization, Methodology, Validation, Formal Analysis, Investigation, Data Curation, Visualization, Writing—Original Draft. JL: Methodology, Validation, Data Curation. YT: Methodology, Writing—Review and Editing. HC: Methodology, Validation, Data Curation. JX: Methodology. HZ: Writing—Review and Editing. YY: Supervision. MM: Resources, Writing—Review and Editing. RX: Conceptualization, Resources, Writing—Review and Editing, Supervision, Project Administration, Funding Acquisition. RX is the guarantor of this article.

Funding The authors have not declared a specific grant for this research from any funding agency in the public, commercial or not-for-profit sectors.

Competing interests No, there are no competing interests.

Patient consent for publication Not applicable.

Ethics approval This study involves human participants and was approved by the Ethics Committee of Shanghai Jie Xin Integrated Traditional Chinese and Western Medicine Hospital, Approval Number: Z-S-ZJMSMS-23-08-001. The Medical Ethics Committee of Ningbo University Affiliated People's Hospital, Approval Number: 2023-(scientific research)-043. Participants gave informed consent to participate in the study before taking part.

Provenance and peer review Not commissioned; externally peer reviewed.

Data availability statement All data relevant to the study are included in the article or uploaded as supplementary information.

ORCID iD

Rimo Xi https://orcid.org/0000-0002-9735-4790

REFERENCES

1 Slamon DJ, Clark GM, Wong SG, *et al*. Human breast cancer: correlation of relapse and survival with amplification of the HER-2/neu oncogene. *Science* 1987;235:177–82.
2 Gravalos C, Jimeno A. HER2 in gastric cancer: a new prognostic factor and a novel therapeutic target. *Ann Oncol* 2008;19:1523–9.
3 Janjigian YY, Kawazoe A, Bai Y, *et al*. Pembrolizumab plus trastuzumab and chemotherapy for HER2-positive gastric or gastro-oesophageal junction adenocarcinoma: interim analyses from the phase 3 KEYNOTE-811 randomised placebo-controlled trial. *The Lancet* 2023;402:2197–208.
4 Gupta S, Shukla S. Limitations of Immunotherapy in Cancer. *Cureus* 2022;14:e30856.
5 Zou W. Regulatory T cells, tumour immunity and immunotherapy. *Nat Rev Immunol* 2006;6:295–307.
6 Hirahara K, Liu L, Clark RA, *et al*. The majority of human peripheral blood CD4+CD25highFoxp3+ regulatory T cells bear functional skin-homing receptors. *J Immunol* 2006;177:4488–94.
7 Ghiringhelli F, Puig PE, Roux S, *et al*. Tumor cells convert immature myeloid dendritic cells into TGF-beta-secreting cells inducing CD4+CD25+ regulatory T cell proliferation. *J Exp Med* 2005;202:919–29.
8 Wing K, Onishi Y, Prieto-Martin P, *et al*. CTLA-4 control over Foxp3+ regulatory T cell function. *Science* 2008;322:271–5.
9 Liu W, Wei X, Li L, *et al*. CCR4 mediated chemotaxis of regulatory T cells suppress the activation of T cells and NK cells via TGF-β pathway in human non-small cell lung cancer. *Biochem Biophys Res Commun* 2017;488:196–203.
10 Sugiyama D, Nishikawa H, Maeda Y, *et al*. Anti-ccr4 mab selectively depletes effector-type foxp3+cd4+regulatory t cells, evoking antitumor immune responses in humans. Proceedings of the National Academy of Sciences; 2013:17945–50.
11 Plitas G, Konopacki C, Wu K, *et al*. Regulatory T Cells Exhibit Distinct Features in Human Breast Cancer. *Immunity* 2016;45:1122–34.
12 Ogura M, Ishida T, Hatake K, *et al*. Multicenter Phase II Study of Mogamulizumab (KW-0761), a Defucosylated Anti-CC Chemokine Receptor 4 Antibody, in Patients With Relapsed Peripheral T-Cell Lymphoma and Cutaneous T-Cell Lymphoma. *J Clin Oncol* 2014;32:1157–63.
13 Sakaguchi S, Yamaguchi T, Nomura T, *et al*. Regulatory T cells and immune tolerance. *Cell* 2008;133:775–87.
14 Zengarini C, Guglielmo A, Mussi M, *et al*. A Narrative Review of the State of the Art of CCR4-Based Therapies in Cutaneous T-Cell Lymphomas: Focus on Mogamulizumab and Future Treatments. *Antibodies (Basel)* 2024;13:32.
15 Ono S, Suzuki S, Kondo Y, *et al*. Trametinib improves Treg selectivity of anti-CCR4 antibody by regulating CCR4 expression in CTLs in oral squamous cell carcinoma. *Sci Rep* 2022;12:21678.
16 Yamamoto K, Utsunomiya A, Tobinai K, *et al*. Phase I study of KW-0761, a defucosylated humanized anti-CCR4 antibody, in relapsed

patients with adult T-cell leukemia-lymphoma and peripheral T-cell lymphoma. *J Clin Oncol* 2010;28:1591–8.
17 Kurose K, Ohue Y, Wada H, *et al*. Phase Ia Study of FoxP3+ CD4 Treg Depletion by Infusion of a Humanized Anti-CCR4 Antibody, KW-0761, in Cancer Patients. *Clin Cancer Res* 2015;21:4327–36.
18 Olkhanud PB, Baatar D, Bodogai M, *et al*. Breast cancer lung metastasis requires expression of chemokine receptor CCR4 and regulatory T cells. *Cancer Res* 2009;69:5996–6004.
19 Kontermann RE, Brinkmann U. Bispecific antibodies. *Drug Discov Today* 2015;20:838–47.
20 Labrijn AF, Janmaat ML, Reichert JM, *et al*. Bispecific antibodies: a mechanistic review of the pipeline. *Nat Rev Drug Discov* 2019;18:585–608.
21 Doi T, Muro K, Ishii H, *et al*. A Phase I Study of the Anti-CC Chemokine Receptor 4 Antibody, Mogamulizumab, in Combination with Nivolumab in Patients with Advanced or Metastatic Solid Tumors. *Clin Cancer Res* 2019;25:6614–22.
22 Ishikawa F, Yasukawa M, Lyons B, *et al*. Development of functional human blood and immune systems in NOD/SCID/IL2 receptor {gamma} chain(null) mice. *Blood* 2005;106:1565–73.
23 Shultz LD, Ishikawa F, Greiner DL. Humanized mice in translational biomedical research. *Nat Rev Immunol* 2007;7:118–30.
24 Kalberer CP, Siegler U, Wodnar-Filipowicz A. Human NK cell development in NOD/SCID mice receiving grafts of cord blood CD34+ cells. *Blood* 2003;102:127–35.
25 Chen J, Liao S, Xiao Z, *et al*. The development and improvement of immunodeficient mice and humanized immune system mouse models. *Front Immunol* 2022;13:1007579.
26 Huntington ND, Legrand N, Alves NL, *et al*. IL-15 trans-presentation promotes human NK cell development and differentiation in vivo. *J Exp Med* 2009;206:25–34.
27 Fridman WH, Pagès F, Sautès-Fridman C, *et al*. The immune contexture in human tumours: impact on clinical outcome. *Nat Rev Cancer* 2012;12:298–306.
28 Ladoire S, Arnould L, Apetoh L, *et al*. Pathologic complete response to neoadjuvant chemotherapy of breast carcinoma is associated with the disappearance of tumor-infiltrating foxp3+ regulatory T cells. *Clin Cancer Res* 2008;14:2413–20.
29 Park S, Jiang Z, Mortenson ED, *et al*. The therapeutic effect of anti-HER2/neu antibody depends on both innate and adaptive immunity. *Cancer Cell* 2010;18:160–70.
30 Bates GJ, Fox SB, Han C, *et al*. Quantification of regulatory T cells enables the identification of high-risk breast cancer patients and those at risk of late relapse. *J Clin Oncol* 2006;24:5373–80.
31 Yoshie O, Matsushima K. CCR4 and its ligands: from bench to bedside. *Int Immunol* 2015;27:11–20.
32 Maeda S, Murakami K, Inoue A, *et al*. CCR4 Blockade Depletes Regulatory T Cells and Prolongs Survival in a Canine Model of Bladder Cancer. *Cancer Immunol Res* 2019;7:1175–87.
33 Salama P, Phillips M, Grieu F, *et al*. Tumor-infiltrating FOXP3+ T regulatory cells show strong prognostic significance in colorectal cancer. *J Clin Oncol* 2009;27:186–92.
34 Mizukami Y, Kono K, Kawaguchi Y, *et al*. CCL17 and CCL22 chemokines within tumor microenvironment are related to accumulation of Foxp3+ regulatory T cells in gastric cancer. *Int J Cancer* 2008;122:2286–93.
35 Fu J, Xu D, Liu Z, *et al*. Increased regulatory T cells correlate with CD8 T-cell impairment and poor survival in hepatocellular carcinoma patients. *Gastroenterology* 2007;132:2328–39.
36 Powell DJ Jr, Felipe-Silva A, Merino MJ, *et al*. Administration of a CD25-directed immunotoxin, LMB-2, to patients with metastatic melanoma induces a selective partial reduction in regulatory T cells in vivo. *J Immunol* 2007;179:4919–28.
37 Zhang A, Fan T, Liu Y, *et al*. Regulatory T cells in immune checkpoint blockade antitumor therapy. *Mol Cancer* 2024;23:251.
38 Hipp S, Tai Y-T, Blanset D, *et al*. A novel BCMA/CD3 bispecific T-cell engager for the treatment of multiple myeloma induces selective lysis in vitro and in vivo. *Leukemia* 2017;31:1743–51.
39 Burt R, Warcel D, Fielding AK. Blinatumomab, a bispecific B-cell and T-cell engaging antibody, in the treatment of B-cell malignancies. *Hum Vaccin Immunother* 2019;15:594–602.
40 Linke R, Klein A, Seimetz D. Catumaxomab. *MAbs* 2010;2:129–36.
41 Zhang A, Ren Z, Tseng K-F, *et al*. Dual targeting of CTLA-4 and CD47 on T_{reg} cells promotes immunity against solid tumors. *Sci Transl Med* 2021;13:eabg8693.
42 Chen Y, Jia M, Wang S, *et al*. Antagonistic Antibody Targeting TNFR2 Inhibits Regulatory T Cell Function to Promote Anti-Tumor Activity. *Front Immunol* 2022;13:835690.
43 Arce Vargas F, Furness AJS, Litchfield K, *et al*. Fc Effector Function Contributes to the Activity of Human Anti-CTLA-4 Antibodies. *Cancer Cell* 2018;33:649–63.
44 Kumar S, Ghosh S, Sharma G, *et al*. Preclinical characterization of dostarlimab, a therapeutic anti-PD-1 antibody with potent activity to enhance immune function in in vitro cellular assays and in vivo animal models. *MAbs* 2021;13:1954136.
45 Perdomo-Celis F, Medina-Moreno S, Davis H, *et al*. HIV Replication in Humanized IL-3/GM-CSF-Transgenic NOG Mice. *Pathogens* 2019;8:33.